Terahertz quantum-cascade lasers

Six years after their birth, terahertz quantum-cascade lasers can now deliver milliwatts or more of continuous-wave coherent radiation throughout the terahertz range — the spectral regime between millimetre and infrared wavelengths, which has long resisted development. This paper reviews the state-of-the-art and future prospects for these lasers, including efforts to increase their operating temperatures, deliver higher output powers and emit longer wavelengths.

BENJAMIN S. WILLIAMS

University of California at Los Angeles, Department of Electrical Engineering, Los Angeles, California 90095-1594, USA

e-mail: bwilliam@ee.ucla.edu

The terahertz frequency range, loosely defined as the frequencies from 300 GHz to 10 THz, or the wavelengths from 30 μm to 1,000 μm, has historically been characterized by a relative lack of convenient radiation sources, detectors and transmission technology. It remains one of the least developed spectral regions, although a surge of activity in the past decade has advanced its potential for applications including but not limited to: astrophysics and atmospheric science, biological and medical sciences, security screening and illicit material detection, non-destructive evaluation, communications technology, and ultrafast spectroscopy. Greatly desired for many applications is a compact, coherent, continuous-wave (c.w.) solid-state source, analogous to the semiconductor laser diode in the visible and infrared, or to transistor oscillators and amplifiers in the microwave. However, at high frequencies the power generated by solid-state electronic devices, such as transistors, Gunn oscillators and Schottky diode multipliers, rolls off owing to both transit-time and resistance–capacitance effects[1,2], and even for the best devices, the available power generated above 1 THz is generally well below the milliwatt level (for example, 50 μW at 1.8 THz for a Schottky multiplier chain)[3,4].

Photonic approaches to direct terahertz generation are limited by the lack of appropriate materials with sufficiently small bandgaps: for example the longest wavelength lead salt laser diodes do not extend below 15 THz. Despite these limitations, a wide variety of techniques have been developed to generate radiation above 1 THz, many, for example, based on down-conversion from the visible regime by using nonlinear or photoconductive effects, or by multiplication up from the millimetre-wave regime, or through direct generation, such as with optically pumped molecular gas lasers or free-electron lasers. Although many of these sources are very useful, they each have their own limitations. Some are inherently limited to pulsed operation, many are limited in output power or require extensive cryogenic cooling, and others are limited by their size, cost or complexity. And so the search for the 'perfect' terahertz source continues. (An extensive review of terahertz sources and applications is beyond the scope of this paper, but there have been several excellent reviews in recent years[1,5,6], as well as several books[7–9].)

The semiconductor-laser model for terahertz generation is an appealing one, given their success and ubiquity throughout the visible and near-infrared frequency range. Because of the lack of appropriate interband materials, in the past, semiconductor terahertz lasers have relied on more exotic gain mechanisms, such as impurity-state-transition lasers[10], or the p-Ge hot-hole laser[11,12]. In this context, the idea of using artificially engineered materials to obtain the desired transitions has seemed a natural route for terahertz devices. In 1971 Kazarinov and Suris proposed amplification by means of stimulated emission of electrons between quantized subbands in two-dimensional quantum wells that could be obtained by growing atomically sharp semiconductor heterostructures[13]. Indeed, many of the early proposals for intersubband lasers focused on generation of radiation with photon energies below the longitudinal-optical (LO) phonon energy (E_{LO} = 36 meV in GaAs, equivalent to 8.7 THz)[14,15]. At low temperatures, electrons in the upper subband would possess insufficient energy to emit an LO-phonon and relax to the lower radiative state; this suppression would result in a relatively long upper-state lifetime, and would ease the task of obtaining a population inversion between levels. Furthermore, the first experimental observations of intersubband emission in 1988 took place in the terahertz[16], perhaps belying the difficulty in demonstrating a terahertz quantum-cascade (QC) laser. The first QC laser was demonstrated at the much shorter wavelength of 4 μm (75 THz) at Bell Labs in 1994 (ref. 17). Since then QC lasers have become the dominant mid-infrared semiconductor laser sources, with spectral coverage from wavelengths of λ = 3–24 μm (refs18–20); room-temperature, c.w. operation with hundreds of milliwatts has been demonstrated for many lasers in the ever-expanding 'sweet-spot' from 3.8–10.6 μm (refs 21,22).

It was in October of 2001 that the first QC laser with a photon energy less than the semiconductor optical phonon energy was demonstrated at 4.4 THz (equivalent to a wavelength of 67 μm) by Köhler *et al.* at the Scuola Normale Superiore in Pisa, Italy, in a collaboration with Cambridge University[23]. In fact, several groups were pursuing this goal, and terahertz lasers were reported soon afterwards by the University of Neuchâtel/Cambridge collaboration[24], the MIT/Sandia collaboration[25], and still others since then[26–32]. Although these first devices lased only in pulsed mode with peak powers of a few milliwatts and ceased lasing above temperatures of several tens of kelvin, intensive research over the past few years has produced rapid improvements. At present, spectral coverage has been demonstrated from 0.84–5.0 THz (refs 33–35), at maximum temperatures up to 169 K, pulsed, and 117 K, c.w. (ref. 36), and output powers of up to 250 mW, pulsed, and 130 mW, c.w. (ref. 37) — although unfortunately these figures are not all from the same device. A survey of the temperature and

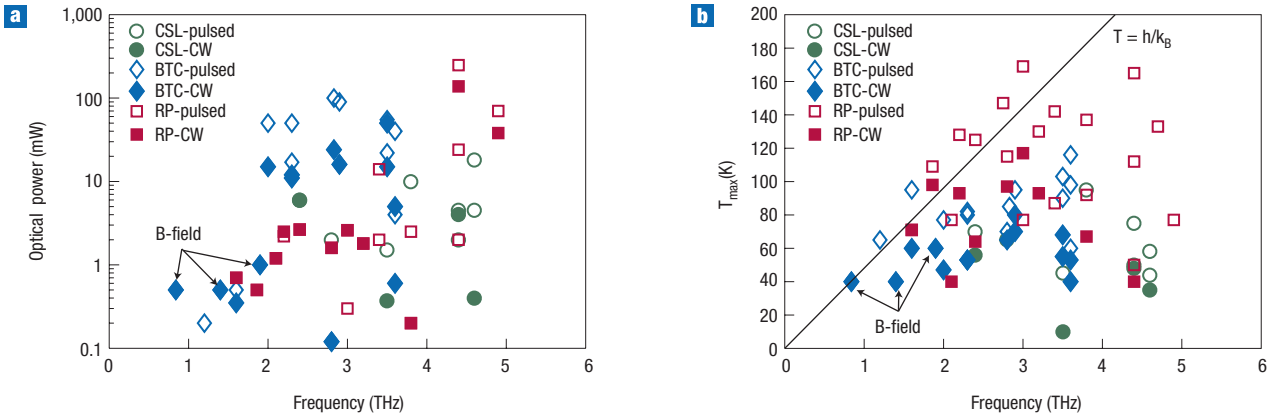

Figure 1 Survey of the reported peak performance of terahertz QC lasers. **a**, Peak optical power and, **b**, peak operating temperatures are shown as a function of lasing frequency. Data are sorted by pulsed or c.w. performance and active-region design: RP, BTC or CSL. Several of the low-frequency designs operate with the assistance of a magnetic field (B-field).

power performance for various devices reported in the literature is illustrated in Fig. 1, separated according to the various types of active regions that are discussed below. Although terahertz-QC-laser development is still progressing at a rapid pace, just past the five-year mark, it seems a reasonable time to take stock of the field, and to identify applications and future research directions.

The task of demonstrating long-wavelength QC lasers proved to be considerably more difficult than the mid-infrared for two reasons. First, because terahertz photon energies are small ($h\nu \approx 4$–20 meV), it is difficult to selectively inject and remove electrons, either by tunnelling or scattering, from such closely spaced subbands so as to achieve the population inversion necessary for gain. Second, as losses due to the absorption of radiation by free carriers increase proportionally to the square of the wavelength, waveguides are required that minimize the modal overlap with any doped semiconductor cladding layers. In the years following the first demonstration of mid-infrared QC lasers, many groups attacked the problem of designing terahertz intersubband emitters, and indeed electroluminescence (but not gain) was observed in a wide variety of structures[38–46]. The breakthrough came in 2001, when Alessandro Tredicucci's group at Pisa demonstrated a terahertz QC laser with a chirped superlattice active region, using a semi-insulating surface-plasmon (SI-SP) waveguide (see below) — the first time a QC structure with significant terahertz gain was paired with a low-loss waveguide[23]. With this introduction, let us consider the various designs for multiple quantum-well active regions and waveguides that are used for terahertz QC lasers.

ACTIVE-REGION DESIGN

The multiple-quantum-well active region is usually grown using molecular-beam epitaxy in the GaAs/$Al_xGa_{1-x}As$ material system, and is the heart of any QC laser. To obtain gain for electromagnetic waves at the frequency ν, energy levels, wavefunctions and scattering rates must be properly engineered to provide a population inversion between two states separated by an energy $h\nu$. To compare some of the various active region designs, it is helpful to know that the peak gain for an intersubband transition between levels 2 and 1 is $g(\nu_0) \propto \Delta N f_{21}/\Delta\nu$, where ΔN is the three-dimensional intersubband population inversion, and $\Delta\nu$ is the transition linewidth[47]. The oscillator strength f_{21} is the ratio of the quantum optical strength of the transition to that of a classical electron oscillator. It is proportional to the stimulated-emission cross-section, and depends heavily on the overlap and symmetry of the initial and final wavefunctions. Aside from the chirped superlattice (CSL) active region, two major design classes of active regions have emerged: bound-to-continuum (BTC) and resonant-phonon (RP) designs. In fact, a handful of hybrid 'interlaced' designs have been demonstrated, in which BTC designs have been combined with phonon-assisted depopulation[48,49].

CHIRPED SUPERLATTICE

The CSL active region, shown in Fig. 2a, is based on the coupling of several quantum wells together in a superlattice to create so-called minibands of states when the appropriate electric field is applied. The radiative transition is designed to take place from the lowest state of the upper miniband '2' to the top state of the lower miniband '1' — analogous to a conventional band-to-band transition. Generally speaking, a population inversion is established because scattering of electrons between the tightly coupled states within the miniband (intra-miniband scattering) is favoured over inter-miniband scattering. Thus electrons tend to relax to the bottom of the minibands, leaving the lower radiative state relatively empty. Population inversion is further favoured by a density-of-states argument, that is, the fact that electrons in the upper radiative state '2' can scatter into any of the lower states in the miniband, but photons will probably only be emitted on the 2→1 transition, that is, between band-edge states. Owing to the relatively small widths of the minibands (about 15–20 meV), LO-phonons are not directly involved in the depopulation process, although they are indirectly involved, as spontaneous emission of LO-phonons is the dominant channel by which the electron gas cools[51].

BOUND-TO-CONTINUUM

The original CSL design has given way to the BTC design (Fig. 2b); the lower radiative state and miniband-based depopulation remains the same, but the upper radiative state is essentially made to be a bound 'defect' state in the minigap[52,53]. The effect is a radiative transition, which is more diagonal in real space. Compared with a CSL design, the oscillator strength of the transition drops slightly (from $f_{21} \approx 2.5$–3 to $f_{21} \approx 1.5$–2), as the overlap with the miniband states drops, but the upper-state lifetime increases as non-radiative scattering is similarly reduced. The injection process also becomes more selective, as the injector states couple more strongly with the upper state than with the lower miniband. As a result, these designs displayed improved temperature and power performance compared with the CSL designs (see Fig. 1, ref. 29,53).

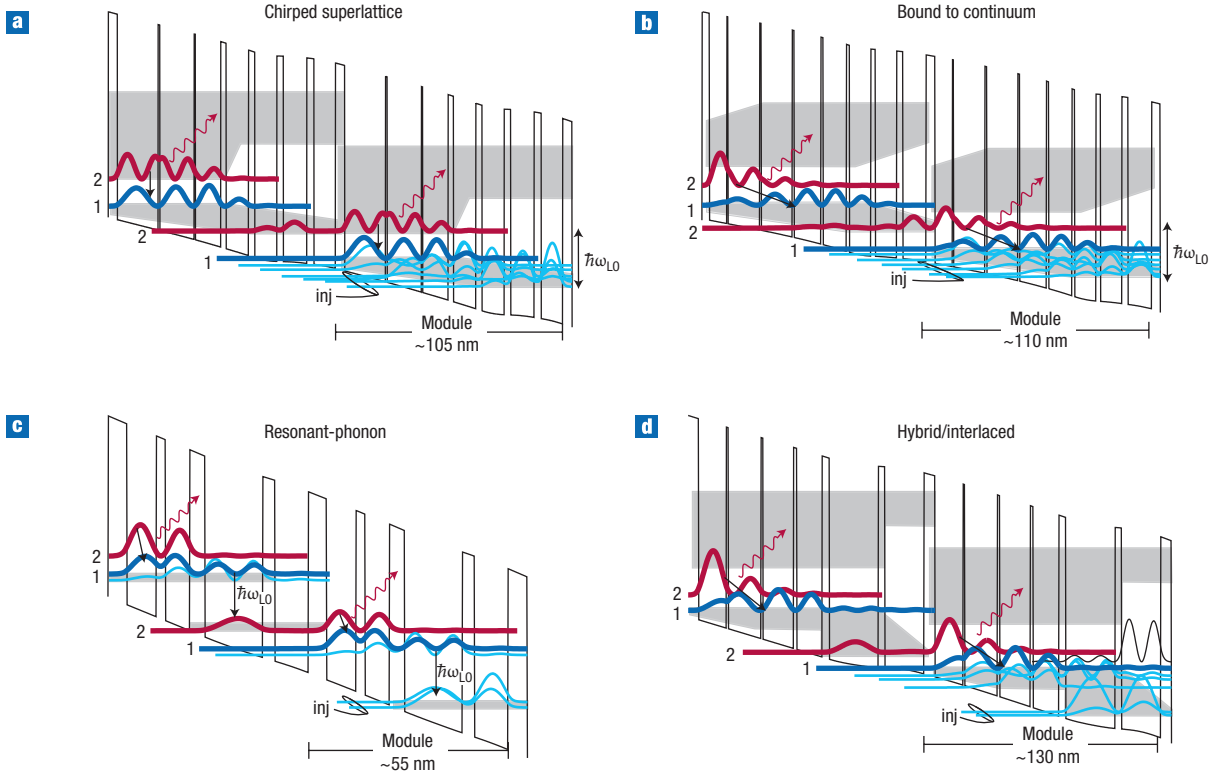

Figure 2 Conduction-band diagrams for major terahertz QC design schemes. Examples are shown for: **a**, CSL, **b**, BTC, **c**, RP and **d**, hybrid/interlaced designs. Two identical modules of each are shown here, although typically 100–200 cascaded modules are grown to form active regions 10–15-μm thick. The squared magnitude of the wavefunctions for the various subband states are plotted, with the upper- and lower-radiative state shown in red and blue respectively and the injector states specifically labelled.The grey shaded regions correspond to minibands of states.

RESONANT-PHONON

The other major active region type is the RP scheme (shown in Fig. 2c, refs 25,54,55). As is common for most mid-infrared QC lasers, collector and injector states are designed to be below the lower radiative state '1' by approximately $E_{LO} = 36$ meV, so that electrons in the lower state will scatter very quickly into the injector states by emitting an LO-phonon. Many early terahertz QC emitter designs suffered from a fundamental difficulty: because of the close subband energy spacing, it was difficult to use LO-phonon scattering to depopulate the lower radiative state without also depopulating the upper state[38,39]. The key development of the RP scheme was bringing the lower radiative state into a broad tunnelling resonance with the excited state in the adjacent quantum wells, so that its wavefunction is spread over several quantum wells. As a result, the lower radiative state maintains a strong spatial overlap with the injector states and experiences subpicosecond LO-phonon scattering. The upper state '2', however, remains localized and has very little overlap with the injector states, which suppresses scattering to the injector states and preserves a lifetime of several picoseconds. The lack of a miniband means that RP designs tend to have a smaller oscillator strength ($f_{21} \approx 0.5$–1) than the BTC designs, but this is partially compensated by the fact that the length L_{mod} of an RP module is typically half that of a BTC module, which results in a higher density of gain producing transitions (that is, $g \propto L_{mod}^{-1}$, ref. 47). In addition, hybrid structures have been developed in which phonon-assisted depopulation has been incorporated with a BTC optical transition (Fig. 2d). These are often known as 'interlaced' structures, owing to alternating photon- and phonon-emission events. Their impact has been limited, but they are particularly notable for achieving very long wavelength operation.

WAVEGUIDES

Because of the strong absorption owing to free carriers at long wavelengths, unique waveguides for terahertz QC lasers have been developed so as to minimize the overlap of the mode with any doped cladding layers. There are two types of waveguides used at present for terahertz QC lasers: the semi-insulating surface-plasmon (SI-SP), and the metal–metal (MM) waveguide, as shown in Fig. 3. It is useful to characterize a laser waveguide by its loss coefficient α_w, which accounts for scattering and absorption inside the waveguide, its confinement factor Γ, which describes the overlap of the mode with the active region, and the mirror loss coefficient α_m, which accounts for losses due to optical coupling, usually owing to finite facet reflectivities. These factors determine the required gain g_{th} to reach the lasing threshold, where the modal gain must equal the total losses: $\Gamma g_{th} = \alpha_w + \alpha_m$.

The SI-SP waveguide involves the growth of a thin (0.2–0.8 μm thick) heavily doped layer underneath the 10-μm-thick active region, but on top of a semi-insulating GaAs substrate[23,24,56]. The result is a compound surface-plasmon mode bound to the top metal contact and the lower plasma layer. Although the mode extends substantially into the substrate, the overlap with any doped semiconductor is small, so that the free-carrier loss is minimized. The confinement factor typically lies in the range $\Gamma = 0.1$–0.5, and in general, modes are somewhat loosely confined, which enables there to be relatively wide ridges without supporting multiple lateral modes. The downside is that ridges narrower than about 100 μm tend to squeeze the mode into the substrate, which limits the minimum device area[57].

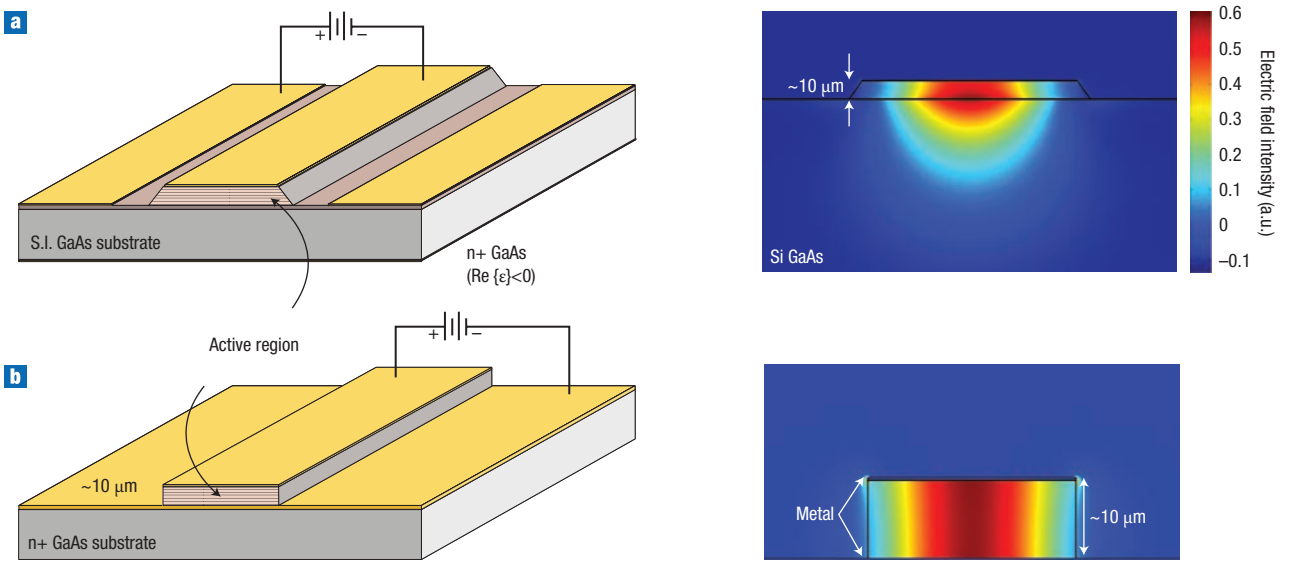

Figure 3 Terahertz QC-laser waveguides. Schematic diagram (left) and typical two-dimensional mode intensity pattern (right) for **a**, SI-SP and **b**, MM waveguides. n+ indicates heavily doped and Re(ε)<0 indicates that the real part of the permittivity is less than zero.

The alternative to the SI-SP, the MM waveguide, uses metal layers, which are placed immediately above and below the epitaxial active region by metallic wafer-bonding to obtain a mode almost completely confined to the active region ($\Gamma \approx 1$, refs 36,50,58,59). After wafer-bonding and substrate removal, the remaining approximately 10-μm-thick epitaxial active region is patterned by photolithography and typically etched into ridges to produce a structure similar to a microstrip transmission line. As any doped contact layers are usually quite thin, waveguide losses are dominated by absorption in the metal, and any re-absorption from inside the active region itself (which is often not negligible).

At present, MM waveguides tend to have the best high-temperature performance, and SI-SP waveguides have higher output powers and better beam patterns. Despite their differences in mode confinement, the scaled waveguide loss α_w/Γ, which determines the lasing threshold, is of similar magnitude for both, or even slightly better for MM waveguides. However, because of the impedance mismatch of the subwavelength mode at the waveguide facet with free-space propagating modes, MM waveguides exhibit enhanced facet reflectivities of $R = 0.5–0.9$ (depending on the waveguide dimensions relative to the wavelength), which is much higher than the expected Fresnel value of $R = 0.32$ calculated from the index mismatch[57]. As a result, MM waveguides are characterized by relatively small mirror losses, and they often exhibit smaller threshold current densities J_{th} and higher operating temperatures[36,37,49], although some other groups have observed little difference in J_{th} between the two types[30]. Furthermore, the strong mode confinement of MM waveguides enables both the vertical and lateral dimensions to be made smaller than the wavelength. This in turn reduces the total thermal dissipation and required cooling power, which enables improved c.w. operation (up to 117 K, refs 30,36).

At the moment, cavity engineering beyond basic Fabry–Pérot configurations is an active area of research. For robust single-mode operation, distributed-feedback resonators can be readily fabricated by patterning or opening apertures in the metal contact to interrupt propagation of the SP mode[60–65], such as shown in Fig. 4a. Recent work has focused on demonstrating MM-waveguide-based microcavities with modal volumes on the order of λ^3, where only a few modes are supported, and threshold currents can be reduced to a few milliamps[66–68]. An example of such a cavity is shown in Fig. 4b. The long wavelength of terahertz radiation means that microcavities can be readily fabricated with photolithography. In addition, field enhancements associated with the cavity structure can maximize nonlinear effects. A notable example is the generation of terahertz sidebands on a $\lambda \approx 1.55$ μm laser carrier, performed by passing the optical signal through the MM-waveguide cavity of a terahertz QC laser, which enables detection of the terahertz signal using conventional telecom technology[69,70].

Unfortunately, the subwavelength nature of MM waveguides causes several difficulties, in particular poor beam patterns and low output powers. As the free-space wavelength is typically between 60 μm and 200 μm, the output beam diffracts nearly omnidirectionally from the facet (typically 10 μm high), which leads to highly divergent beam patterns, often with interference fringes[71,72]. Furthermore, because the mirror losses ($\alpha_m = 1–2$ cm^{-1}) are much smaller than the waveguide losses ($\alpha_w = 10–20$ cm^{-1}), only a small fraction (5–20%) of the generated photons escape the cavity without being reabsorbed. In other words, most MM-waveguide lasers operate far from the optimum coupling condition and radiate only milliwatts of terahertz power[73], of which only a fraction is collected owing to the beam divergence. In comparison, the large mode size of SI-SP waveguides results in a less-divergent beam[74,75], and a more favourable ratio of mirror losses to waveguide losses yields higher output powers and efficiencies. The highest output powers from terahertz QC lasers have been observed using SI-SP waveguides, such as 248 mW (pulsed) with an RP active region[37], and about 100 mW (pulsed) with BTC active regions[29,32,76]. In fact, recent thermal analysis of a BTC device using a microprobe photoluminescence method suggests that poor collection efficiency has been hampering power measurements, and in fact a value of 5.5% for the wall-plug efficiency at 40 K was extracted, the highest value yet reported[32].

Because of the superior temperature performance of MM-waveguide devices, there are many efforts underway at present to improve their optical coupling efficiency and beam patterns. One solution is to micromachine a mode-matching device such as a horn antenna, similar to those used widely with microwave and

millimetre-wave devices. Although the fabrication is challenging, preliminary results have reported improvements to the collected power by a factor of ten[77]. Some research groups have focused on surface emission from MM waveguides using broad-area second-order distributed-feedback structures[27,64] and two-dimensional photonic crystals[78]. Ideally, proper design of the feedback structure would enable engineering of the surface coupling to optimize the lasing threshold, beam pattern and output power. Single-mode operation with a narrowed beam pattern has been observed by several groups, but achieving optimum performance has been complicated by issues such as higher-order lateral modes and strong facet reflections. An alternative approach is to place a silicon hyperhemispherical lens next to the facet of an MM waveguide — this serves the dual purpose of reducing the facet reflectivity through index matching and better collimating the emitted radiation. This scheme was used to boost the peak pulsed output power of a 4.1-THz MM-waveguide laser by more than a factor of five up to 145 mW (at 10 K), while only reducing the maximum lasing temperature from 165 K to 160 K (ref. 73). For all of these schemes, the fact that the output power can be increased so substantially without significantly increasing the threshold J_{th} suggests that further efficiency gains are possible.

HIGH-TEMPERATURE PERFORMANCE

Although the first terahertz QC laser operated only up to a maximum temperature of T_{max} = 40 K (ref. 23), improvements in active regions and waveguides have brought previously unavailable performance: milliwatts of c.w. power at the temperature of liquid nitrogen (77 K) from a semiconductor laser, with T_{max} up to 169 K in pulsed mode at 2.9 THz. The next milestone is operation at temperatures accessible by thermoelectric coolers (about 240 K) or even better, at room temperature.

There are two major processes that are expected to cause the degradation of population inversion (and thus gain) in terahertz QC lasers at higher temperatures: thermal backfilling and thermally activated phonon scattering. A schematic of these processes is shown in Fig. 5b. Backfilling of the lower radiative state with electrons from the heavily populated injector occurs either by thermal excitation (according to the Boltzmann distribution), or by reabsorption of non-equilibrium LO-phonons (the hot-phonon effect)[79]. The other principal degradation mechanism is the onset of thermally activated LO-phonon scattering, as electrons in the upper subband acquire sufficient in-plane kinetic energy to emit an LO-phonon and relax to the lower subband. This causes the upper-state lifetime τ_{21} to decrease exponentially according to $\tau_{21}^{-1} \propto \exp[-(E_{LO} - h\nu)/k_B T_e]$, where $h\nu$ is the terahertz photon energy, and k_B is the Boltzmann constant. Both of these mechanisms sensitively depend on the electron gas temperature T_e, which Monte Carlo simulations as well as microprobe photoluminescence measurements suggest is 50–100 K higher than the lattice temperature during device operation[80,81]. The temperature dependence of waveguide losses is also not well understood, but recent experiments that apply the powerful technique of broadband time-domain terahertz spectroscopy to measure loss and gain in QC lasers during operation should provide a better understanding of absorption mechanisms, as well as gain and transport dynamics[82].

In general, RP designs have better temperature performance than BTC designs. Well-designed RP lasers with MM waveguides regularly operate above 130 K and even as high as 169 K (refs 28,36,83), whereas BTC designs tend to top out around 100–115 K (refs 29,49,53). The explicit inclusion of an LO-phonon scattering event for depopulation means that RP designs present a larger energetic barrier (about 36 meV) to thermal backfilling than most BTC designs (about 15–20 meV). Although this excess-voltage defect hurts the wall-plug efficiency of RP designs at very low temperatures, it appears to be an advantage for higher-temperature operation.

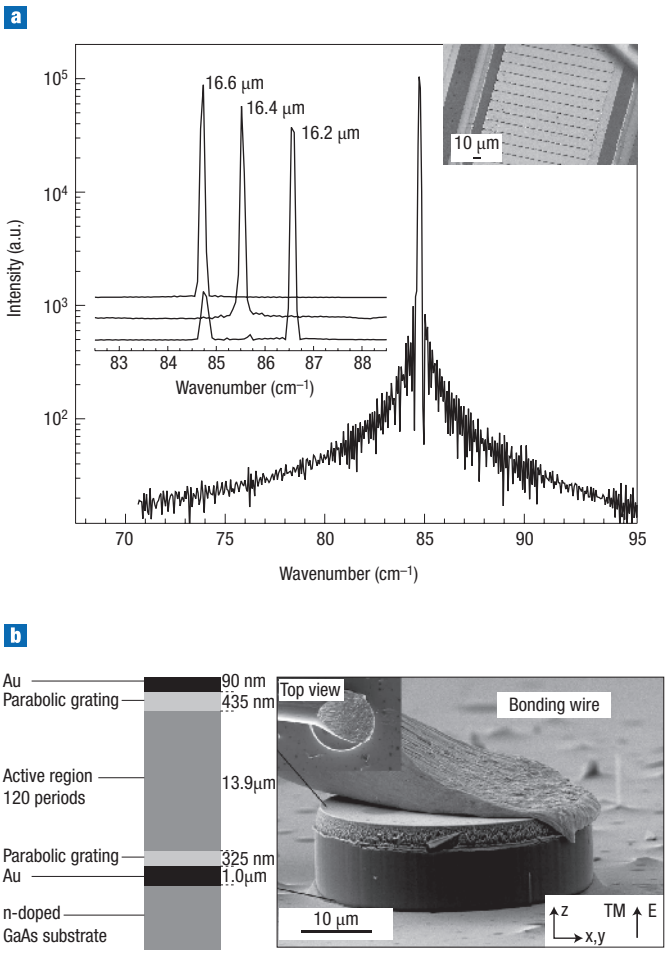

Figure 4 Various terahertz cavities. **a**, Log-scale single-mode emission spectrum of a 2.2-mm-long didtributed-feedback SI-SP laser with a slit periodicity of 16.5 μm. The left inset shows linear-scale spectra of three lasers with different slit periodicities (as indicated). The right inset shows a scanning electron microscope image of the structure. Reproduced with permission from ref. 60. Copyright (2005) AIP. **b**, Left, a schematic of the vertical structure of a 40-μm-diameter MM-waveguide microdisk cavity. Right, a scanning electron microscope image of the structure. (E_{TM} indicates the direction of the transverse-magnetic electric field with respect to the *x* and *z* axes.) Reproduced with permission from ref. 66. Copyright (2007) AIP.

For present RP designs, practical transport considerations play a major role in limiting temperature performance, because for a given design, the temperature range is largely determined by the dynamic range between the J_{th} and the maximum current density J_{max}. When J_{max} is reached, subband misalignment occurs and the device exhibits negative differential resistance (see Fig. 5a). This can be seen by examination of plots of J_{th} versus temperature for three exemplar devices at different frequencies in Fig. 5b. In general, devices with lower $h\nu$ exhibit a weaker increase in J_{th} with temperature, probably owing to the larger energy barrier, $E_{LO} - h\nu$, for thermally activated phonon scattering. However, lower-frequency devices tend to have a smaller dynamic range for lasing, a consequence of reduced injection and depopulation selectivity that results from the very closely spaced energy levels. Improvements in designs to reduce subthreshold parasitic current channels that limit reductions in J_{th}, and to raise the maximum current, will continue to

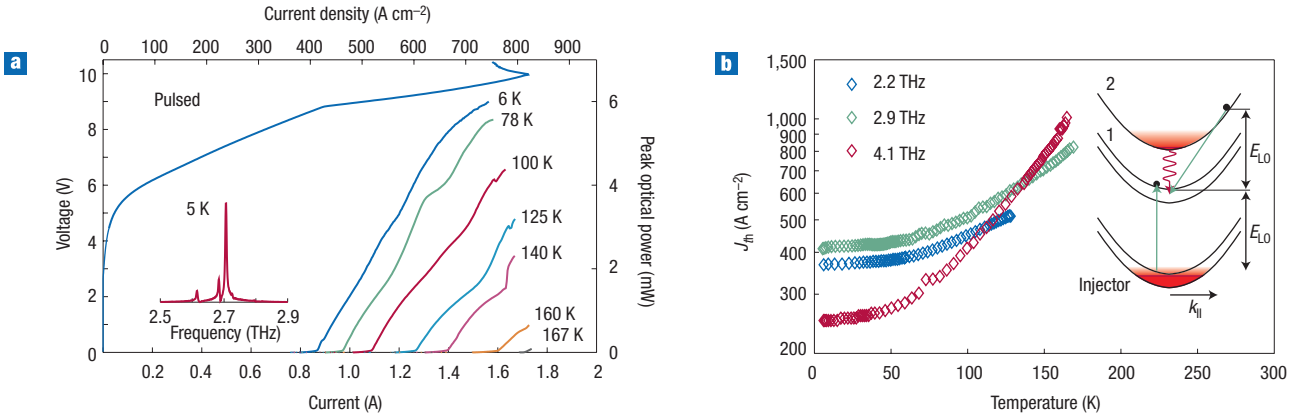

Figure 5 High-temperature performance. **a**, Optical power and voltage versus current characteristics in pulsed mode. Inset shows a typical measured spectral intensity for an RP device with an MM waveguide in pulsed mode. **b**, Threshold current density versus temperature in pulsed mode for several RP devices with MM waveguides at different frequencies. The inset shows a schematic of the subband in-plane dispersion diagram for an RP device, with the two major temperature degradation processes illustrated (green arrows). $k_{||}$ is the in-plane wave number. (Data are courtesy of Q. Hu).

improve temperature performance of current designs, especially at lower frequencies where the dynamic range is particularly limited.

It is interesting to note that several of the reported lasers (see Fig. 1) operate at temperatures such that the lattice thermal energy is greater than the photon energy ($k_BT > h\nu$). However, we should not be overly concerned by this — there is no fundamental limit associated with this condition, and in fact the electron gas is hotter still. As a laser is a non-equilibrium system, as long as a favourable lifetime ratio $\tau_{21}/\tau_1 > 1$ (where τ_1 is the lower state lifetime) can be engineered (no easy feat), a population inversion of some magnitude will exist between the radiative states.

LONG-WAVELENGTH LASERS

Since the demonstration of the first terahertz QC laser at 4.4 THz, there has been a strong interest in demonstrating terahertz QC lasers at ever lower frequencies. Although this is partly motivated by the desire to maximize the spectral coverage of QC lasers, many materials, such as explosives and drugs, have relevant spectral features in the 1–2 THz range[84–87], and many other materials, such as water, clothing and the atmosphere, become more transparent[88,89], owing to both reduced absorption and scattering. At present, performance in terahertz QC lasers degrades significantly below 2.5 THz (see Fig. 1), with the lowest reported frequencies (without a magnetic field) being 1.59 THz from an RP design[90], and 1.2 THz from a hybrid BTC design[50]. The barriers to achieving very-low-frequency operation are simply more extreme versions of the difficulties associated with all terahertz QC lasers: the small subband energy separations and higher free-carrier losses. To generate a 1-THz photon requires 4-meV subband separation, which is approaching the intersubband level broadening; this dephasing of the transition may set an eventual lower limit on the emission frequency. Transport difficulties arise even before this point, however. With many other subbands nearby in energy space, it becomes increasingly difficult to selectively inject carriers to the correct level, and parasitic coupling to other levels increases at the expense of gain. Preventing this is a major focus of design efforts[90].

At low frequencies, a large concern is the absorption at $h\nu$ caused by the high-energy tails of the intersubband transitions inside the injector miniband. To address this issue, modified BTC structures (shown in Fig. 2d) have replaced their many-level injector manifold with a doublet state, and achieved frequencies of 1.6 THz (ref. 50), and less even down to 1.2 THz ($\lambda = 250$ μm, reported by C. Walther, M. Fischer, G. Scalari, & J. Faist, unpublished results). The energy splitting of this doublet is a very narrow 1–2 meV, which helps to keep the intersubband resonance smaller than the photon energy, which is as low as 5 meV for 1.2 THz. It is also possible to reduce the injector to a single state, thus eliminating any intersubband transitions inside the injector[83,90]. Magnetic-field-assisted QC lasers are currently pushing the ultimate long-wavelength limits, where lasing has been demonstrated at 1.39 THz (ref. 34), and more recently as low as 840 GHz ($\lambda = 357$ μm, ref. 33). The formation of Landau levels in high magnetic fields (more than 6 T) effectively quantizes in-plane motion and reduces the phase space for non-radiative scattering. This leads to long upper-state lifetimes and ultralow threshold current densities ($J_{th} < 1$ A cm^{-2} at 10 K, ref. 91). The reduced scattering also leads to narrower intersublevel emission linewidths, and reduced free-carrier absorption, both of which improve gain at low frequencies. Although the magnetic fields required will limit practical applications of these lasers, they are an impressive example of the limits achievable by semiconductor lasers, and suggest the potential advantages in reducing the density of states through additional quantum confinement.

APPLICATIONS

A full examination of the applications of terahertz QC lasers and terahertz radiation in general is far beyond the scope of this article, and has been explored in other review articles and books[1,7,9,88]. Nevertheless, I would like to highlight two applications as examples for which terahertz QC lasers show great promise.

Much of the push for c.w. terahertz sources has historically come from the astrophysics and space-science community, and preliminary work has now been performed by several groups to evaluate the suitability of QC lasers as local oscillator sources for submillimetre-wave heterodyne receivers used to perform high-resolution spectroscopy[1,92,93]. In separate experiments, superconducting hot-electron bolometer mixers were pumped by an RP device in an MM waveguide at 2.8 THz (ref. 94), and by a BTC device in an SI-SP waveguide at 2.5 THz (ref. 74). In both cases, the receiver-noise temperature was found to be just as good or better than when the mixers were pumped by far-infrared gas lasers. Further along these lines, a terahertz QC laser was frequency locked to a gas laser source and displayed a stable time-averaged linewidth of 65 kHz, far in excess of the 10^{-6} relative-frequency

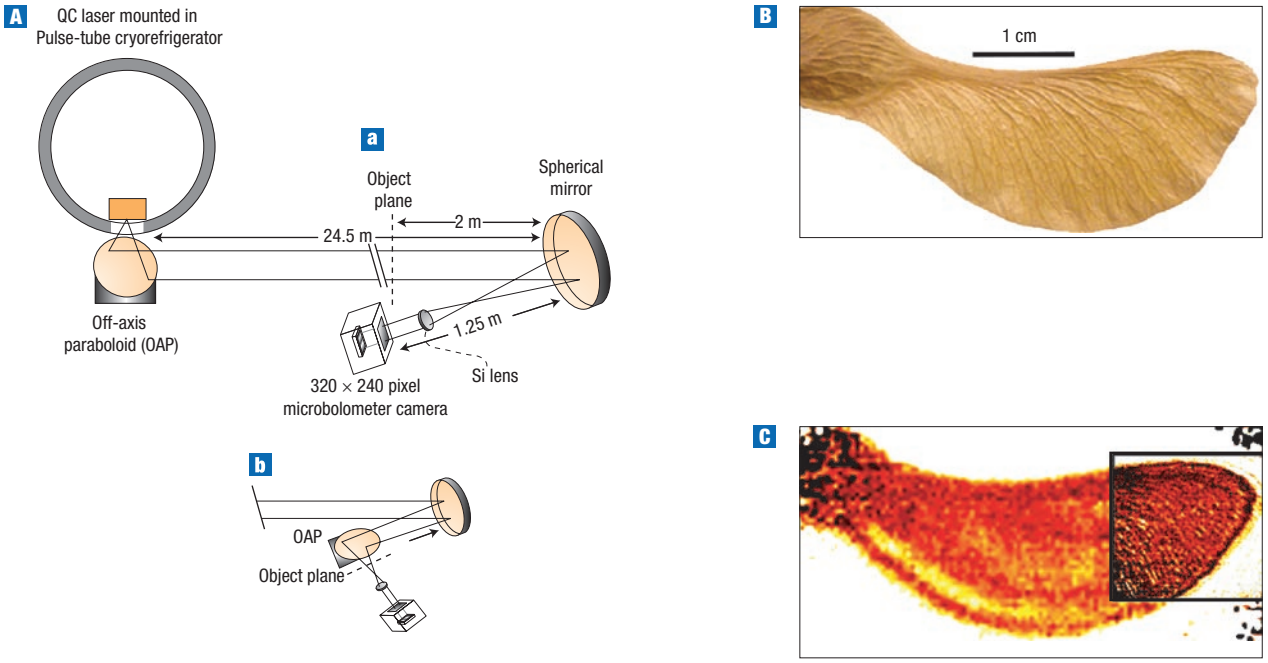

Figure 6 Terahertz imaging with a QC laser. **A**, Experimental set-up for imaging over a distance of 25 m, where a QC laser mounted in a pulse-tube cryocooler is used as the illumination source, and a room-temperature microbolometer focal-plane array camera is used to perform imaging in two possible configurations, **a** and **b**. Also shown is a seed pod visible image, **B**, and terahertz image, **C**, taken with a 1-s integration time in imaging configuration **a**. The inset of **C** shows the terahertz image from configuration **b**. Reproduced with permission from ref. 35. Copyright (2006) AIP.

accuracy necessary for most spectroscopic applications[95]. Several other experiments have measured relatively narrow short-term linewidths (less than 30 kHz over 3-ms sweep time)[96,97]. These narrow linewidths are not surprising, as like all intersubband lasers, these devices are expected to have small-linewidth enhancement factors, and the free running linewidth is determined principally by thermal fluctuations. The critical step of phase-locking a QC laser to a stabilized microwave source has yet to be demonstrated. Further waveguide development is also needed. For example, the superior temperature performance of the MM waveguide, and the ability to drastically reduce the active-region volume and thus minimize the required cooling power, are highly attractive for any local oscillator application. However, the poor beam pattern and phase front observed from Fabry–Pérot MM ridge waveguides severely impedes coupling into the mixer — a fact that gives further incentive to efforts to improve the beam-pattern from MM devices. Also, as single-mode operation is required, distributed-feedback cavities will probably also be needed, although still better would be an implementation of a cavity that enables wideband tunability[98]. Although varying the temperature of the active region has yielded a single-mode tuning range of at most 20 GHz, the prospects for improvement are tantalizing, as measurements suggest an available gain bandwidth of several hundred gigahertz or more[62,64]. In short, local oscillators are sorely needed above 2 THz, and QC lasers seem to be well-suited for the task, although further work remains to be done before they can be considered instrument-ready.

The second major application I would like to highlight is the use of QC lasers as high-average power sources for imaging. Terahertz imaging has received considerable attention, partly because of the fact that many materials such as clothing and packaging are transparent at terahertz wavelengths, leading to possible applications in non-invasive inspection for industrial and pharmaceutical processes, security screening, mail inspection and biomedical imaging among others. Although the majority of the work on terahertz imaging has been performed using broadband ultrafast time-domain spectroscopic methods[7,99], QC laser sources may have a role to play, as they can deliver higher average powers (milliwatt-level compared with microwatt-level), and narrowband sources can more readily take advantage of the (modest) atmospheric transmission windows that are scattered throughout the terahertz regime. Most terahertz imaging using QC lasers has been performed in a single-pixel configuration by mechanically scanning the sample with such detectors as liquid-helium-cooled bolometers, Schottky diode mixers and Golay cells[75,100–102], although more sophisticated tomographic configurations have been used to perform three-dimensional imaging[103]. However, terahertz QC lasers can deliver sufficient average power to illuminate focal-plane arrays of room-temperature direct detectors. Lee *et al.* demonstrated real-time, video-rate, terahertz imaging using an RP QC laser with an SI-SP waveguide in conjunction with a commercial room-temperature microbolometer camera[104]. A 4.3-THz device was cooled to 30 K in a cryogen-free pulsed tube cryocooler to provide the delivery of peak powers of 50 mW at a 33% duty cycle, which enabled a video at 20 frames per second, with signal-to-noise ratios of 20–30 dB — sufficient to enable imaging of pencil writing though envelopes. By taking advantage of a transmission window at 4.9 THz, imaging in transmission mode over a 25-m distance was also possible (shown in Fig. 6, ref. 35). Improved sensitivity could be obtained by optimizing the microbolometer absorber for terahertz (about10 dB improvement), or by moving to cryogenic direct detectors, such as quantum-well infrared photodetectors[105]. Heterodyne detection schemes would provide the ultimate in sensitivity, but are difficult to implement in large-format focal-plane arrays. However, if scanned imaging is acceptable, QC lasers could serve as substitutes for the molecular gas lasers that serve as sources and local oscillators in some of the single-detector heterodyne imaging schemes that have been demonstrated[106,107].

FUTURE OUTLOOK

When talking about terahertz QC lasers, probably the most frequently asked question is: "When will they operate at room temperature?" Indeed, room-temperature lasers would lower the entry barrier for many applications, particularly those where portability or power efficiency (or both) are important. These might include hand-held sensors for detection of explosives or bioagents, environmental gas sensing or semiconductor-wafer inspection. It seems probable that continuing advances with existing designs and epitaxial growth will push operation over 200 K, and perhaps even within the range of thermoelectric coolers at about 240 K, within several years. For example, examination of the J_{th} versus temperature characteristics shown in Fig. 5a suggests that even moderate increases in the current dynamic range could provide significant improvements, particularly for longer-wavelength devices.

In my opinion, room-temperature operation of terahertz QC lasers will require an additional revolution in the field, either through the invention of an alternative active-region design, or more radically, through the use of a new material system. For example, the GaN/AlGaN system has been suggested, because its large LO-phonon energy (about 90 meV) would present a large barrier to thermally activated phonon scattering and backfilling[108,109]. However, material growth and modelling is notoriously difficult in GaN/AlGaN materials, and a GaN-based QC laser has yet to be demonstrated at any wavelength. Even more ambitious are proposals to develop low-threshold, high-temperature, QC structures in zero-dimensional heterostructures (that is, quantum dots or semiconductor nanowires)[110–113]. Like magnetic-field-assisted QC lasers, the additional quantum confinement offers the prospect of suppressed non-radiative LO-phonon scattering — a version of the much debated phonon-bottleneck effect. However, it must be remembered that the successful advent of QC lasers, particularly in the terahertz regime, has depended on the exquisite material control and flexibility of bandgap engineering provided by planar epitaxy, and any new system must satisfy similar criteria.

It would be a mistake to focus exclusively on room-temperature operation as a metric, as there are many applications, such as heterodyne receivers for astronomy, or non-destructive inspection in an industrial setting, where some form of cooling would be acceptable. Terahertz QC lasers are now the brightest c.w. solid-state sources that operate above liquid nitrogen temperatures in the 1.2–5 THz range, and the successful extension of coverage to frequencies below 1 THz is exceeding expectations. In the near future, we can expect that new cavity coupling schemes will provide high-power single-mode terahertz beams from subwavelength MM waveguides that operate in c.w. well above the temperature of liquid nitrogen, and efforts to demonstrate widely tunable terahertz QC lasers promise to be exceedingly active for many years to come. Quantum-cascade lasers are a testament to our ability to engineer the quantum properties of materials, and have now provided a sorely needed convenient source of terahertz radiation. The degree to which the non-trivial challenges that lie ahead for performance and use are met with innovations in design and materials will go a long way to determining their eventual technological impact.

doi:10.1038/nphoton.2007.166

References

1. Siegel, P. H. Terahertz technology. *IEEE Trans. Microwave Theory Tech.* **50,** 910–928 (2002).
2. Woolard, D. L., Brown, E. R., Pepper, M. & Kemp, M. Terahertz frequency sensing and imaging: A time of reckoning future applications? *Proc. IEEE* **93,** 1722–1743 (2005).
3. Mehdi, I. *et al.* Terahertz multiplier circuits in *2006 IEEE MTT-S International Microwave Symposium Digest* 341–344 (IEEE, San Fransisco, California, 2006).
4. Maestrini, A. *et al.* A 1.7–1.9 THz local oscillator source. *IEEE Microwave Wireless Components Lett.* **14,** 253–255 (2004).
5. Tonouchi, M. Cutting-edge terahertz technology. *Nature Photon.* **1,** 97–105 (2007).
6. Ferguson, B. & Zhang, X.-C. Materials for terahertz science and technology. *Nature Mater.* **1,** 26–33 (2002).
7. *Sensing with Terahertz Radiation* (ed. Mittleman, D.) (Springer, Berlin, 2003).
8. *Terahertz Sensing Technology* Vol. 1 (Selected Topics in Electronics and Systems Vol. 30) (eds Woolard, D. L., Leorop, W. R. & Shur, M. S.) (World Scientific, Singapore, 2003).
9. *Terahertz Sensing Technology* Vol. 2 (Selected Topics in Electronics and Systems Vol. 32) (eds Woolard, D. L., Leorop, W. R. & Shur, M. S.) (World Scientific, Singapore, 2004).
10. Hübers, H.-W. *et al.* Terahertz emission spectra of optically pumped silicon lasers. *Phys. Status Solidi (b)* **233,** 191–196 (2002).
11. (eds Gornik, E. & Andronov, A. A , Special issue - Far-infrared semiconductor lasers) *Opt. Quant. Electron.* **23,** (1991).
12. Bründermann, E., Chamberlin, D. R. & Haller, E. E. High duty cycle and continuous terahertz emission from germanium. *Appl. Phys. Lett.* **76,** 2991–2993 (2000).
13. Kazarinov, R. F. & Suris, R. A. Possibility of the amplification of electromagnetic waves in a semiconductor with a superlattice. *Sov. Phys. Semiconductors* **5,** 707–709 (1971).
14. Borenstain, S. I. & Katz, J. Evaluation of the feasibility of a far-infrared laser based on intersubband transitions in GaAs quantum wells. *Appl. Phys. Lett.* **55,** 654–656 (1989).
15. Hu, Q. & Feng, S. Feasibility of far-infrared lasers using multiple semiconductor quantum wells. *Appl. Phys. Lett.* **59,** 2923–2925 (1991).
16. Helm, M., Colas, E., England, P., DeRosa, F. & Allen Jr, S. J. Observation of grating-induced intersubband emission from GaAs/AlGaAs superlattices. *Appl. Phys. Lett.* **53,** 1714–1716 (1988).
17. Faist, J. *et al.* Quantum cascade laser. *Science* **264,** 553–556 (1994).
18. Revin, D. G. *et al.* InGaAs/AlAsSb/InP quantum cascade lasers operating at wavelengths close to 3 μm. *Appl. Phys. Lett.* **90,** 021108 (2007).
19. Semtsiv, M. P., Wienold, M., Dressler, S. & Masselink, W. T. Short-wavelength ($\lambda \approx 3.05$ μm) InP-based strain-compensated quantum-cascade laser. *Appl. Phys. Lett.* **90,** 051111 (2007).
20. Colombelli, R. *et al.* Far-infared surface-plasmon quantum-cascade lasers at 21.5 μm and 24 μm wavelengths. *Appl. Phys. Lett.* **78,** 2620–2622 (2001).
21. Yu, J. S., Evans, A., Slivken, S., Darvish, S. R. & Razeghi, M. Temperature dependent characteristics of $\lambda \sim 3.8\mu$m room-temperature continuous-wave quantum-casacde lasers. *Appl. Phys. Lett.* **88,** 251118 (2006).
22. Slivken, S., Evans, A., Zhang, W. & Razeghi, M. High-power, continuous-operation intersubband laser for wavelengths greater than 10 μm. *Appl. Phys. Lett.* **90,** 151115 (2007).
23. Köhler, R. *et al.* Terahertz semiconductor-heterostructure laser. *Nature* **417,** 156–159 (2002).
24. Rochat, M. *et al.* Low-threshold terahertz quantum-cascade lasers. *Appl. Phys. Lett.* **81,** 1381–1383 (2002).
25. Williams, B. S., Callebaut, H., Kumar, S., Hu, Q. & Reno, J. L. 3.4-THz quantum cascade laser based on longitudinal-optical-phonon scattering for depopulation. *Appl. Phys. Lett.* **82,** 1015–1017 (2003).
26. Liu, H. C. *et al.* Effect of doping concentration on the performance of terahertz quantum-cascade lasers. *Appl. Phys. Lett.* **87,** 141102 (2005).
27. Fan, J. A. *et al.* Surface emitting terahertz quantum cascade laser with a double-metal waveguide. *Opt. Express* **14,** 11672–11680 (2006).
28. Benz, A. *et al.* Influence of doping on the performance of terahertz quantum-cascade lasers. *Appl. Phys. Lett.* **90,** 101107 (2007).
29. Alton, J. *et al.* Optimum resonant tunneling injection and influence of doping density on the performance of THz bound-to-continuum cascade lasers. *Proc. SPIE* **5727,** 65–73 (2005).
30. Dhillon, S. *et al.* Ultralow threshold current terahertz quantum cascade lasers based double-metal buried strip waveguides. *Appl. Phys. Lett.* **87,** 071107 (2005).
31. Tamosiunas, V. *et al.* Terahertz quantum cascade lasers in a magnetic field. *Appl. Phys. Lett.* **83,** 3873–3875 (2003).
32. Vitiello, M. S., Scamarcio, G., Spagnolo, V., Dhillon, S. S. & Sirtori, C. Terahertz quantum cascade lasers with large wall-plug efficiency. *Appl. Phys. Lett.* **90,** 191115 (2007).
33. Faist, J., Scalari, G., Walther, C. & Fischer, M. in *2007 Materials Research Society (MRS) Spring Meeting, San Fransisco, California, April 2007* CC7.2 (2007).
34. Scalari, G., Walther, C., Faist, J., Beere, H. & Ritchie, D. Electrically switchable, two-color quantum cascade laser emitting at 1.39 and 2.3 THz. *Appl. Phys. Lett.* **88,** 141102 (2006).
35. Lee, A. W. M. *et al.* Real-time terahertz imaging over a standoff distance (> 25 meters). *Appl. Phys. Lett.* **89,** 141125 (2006).
36. Williams, B. S., Kumar, S., Hu, Q. & Reno, J. L. Operation of terahertz quantum-cascade lasers at 164 K in pulsed mode and at 117 K in continuous-wave mode. *Opt. Express* **13,** 3331–3339 (2005).
37. Williams, B. S., Kumar, S., Hu, Q. & Reno, J. L. High-power terahertz quantum cascade lasers. *Electron. Lett.* **42,** 89–91 (2006).
38. Xu, B., Hu, Q. & Melloch, M. R. Electrically pumped tunable terahertz emitter based on intersubband transition. *Appl. Phys. Lett.* **71,** 440–442 (1997).
39. Williams, B. S., Xu, B., Hu, Q. & Melloch, M. R. Narrow-linewidth terahertz intersubband emission from three-level systems. *Appl. Phys. Lett.* **75,** 2927–2929 (1999).
40. Williams, B. S., Callebaut, H., Hu, Q. & Reno, J. L. Magnetotunneling spectroscopy of resonant anticrossing in terahertz intersubband emitters. *Appl. Phys. Lett.* **79,** 4444–4446 (2001).
41. Rochat, M., Faist, J., Beck, M., Oesterle, U. & Ilegems, M. Far-infrared ($\lambda = 88$ μm) electroluminescence in a quantum cascade structure. *Appl. Phys. Lett.* **73,** 3724–3726 (1998).
42. Blaser, S., Rochat, M., Beck, M. & Faist, J. Far-infrared emission and stark-cyclotron resonances in a quantum-cascade structure based on photon-assisted tunneling transition. *Phys. Rev. B* **61,** 8369–8374 (2000).
43. Menon, V. M. *et al.* Dual-frequency quantum-cascade terahertz emitter. *Appl. Phys. Lett.* **80,** 2454–2456 (2002).
44. Ulrich, J. *et al.* Terahertz quantum cascade structures: Intra-versus interwell transition. *Appl. Phys. Lett.* **77,** 1928–1930 (2000).
45. Colombelli, R. *et al.* Terahertz electroluminescence from superlattice quantum cascade structures. *J. Appl. Phys.* **91,** 3526–3529 (2002).
46. Ulrich, J., Zobl, R., Unterrainer, K., Strasser, G. & Gornik, E. Magnetic-field-enhanced quantum-cascade emission. *Appl. Phys. Lett.* **76,** 19–21 (2000).

47. Faist, J., Capasso, F., Sirtori, C., Sivco, D. & Cho, A. in *Intersubband transitions in quantum wells: Physics and device applications II* Vol. 66 (eds Liu, H. C. & Capasso, F.) Ch. 1, 1–83 (Academic, San Diego, 2000).
48. Köhler, R. *et al.* Terahertz quantum-cascade lasers based on an interlaced photon-phonon cascade. *Appl. Phys. Lett.* **84,** 1266–1268 (2004).
49. Scalari, G., Hoyler, N., Giovannini, M. & Faist, J. Terahertz bound-to-continuum quantum cascade lasers based on optical-phonon scattering extraction. *Appl. Phys. Lett.* **86,** 181101 (2005).
50. Walther, C., Scalari, G., Faist, J., Beere, H. & Ritchie, D. Low frequency terahertz quantum cascade laser operating from 1.6 to 1.8 THz. *Appl. Phys. Lett.* **89,** 231121 (2006).
51. Shah, J. in *Hot carriers in semiconductor nanostructures* (ed. Shah, J.) Ch. 4, 169–188 (Academic, San Diego, 1992).
52. Faist, J., Beck, M., Aellen, T. & Gini, E. Quantum-cascade lasers based on a bound-to-continuum transition. *Appl. Phys. Lett.* **78,** 147–149 (2001).
53. Scalari, G. *et al.* Far-infrared $\lambda \approx 87$ μm) bound-to-continuum quantum-cascade lasers operating up to 90 K. *Appl. Phys. Lett.* **82,** 3165–3167 (2003).
54. Hu, Q. *et al.* Resonant-phonon-assisted THz quantum-cascade lasers with metal-metal waveguides. *Semicond. Sci. Technol.* **20,** S228–S236 (2005).
55. Stroscio, M. A., Kisin, M., Belenky, G. & Luryi, S. Phonon enhanced inverse population in asymmetric double quantum wells. *Appl. Phys. Lett.* **75,** 3258–3260 (1999).
56. Ulrich, J. *et al.* Terahertz-electroluminescence in a quantum cascade structure. *Physica B* **272,** 216–218 (1999).
57. Kohen, S., Williams, B. S. & Hu, Q. Electromagnetic modeling of terahertz quantum cascade laser waveguides and resonators. *J. Appl. Phys.* **97,** 053106 (2005).
58. Williams, B. S., Kumar, S., Callebaut, H., Hu, Q. & Reno, J. L. Terahertz quantum-cascade laser at $\lambda \approx 100$ μm using metal waveguide for mode confinement. *Appl. Phys. Lett.* **83,** 2124–2126 (2003).
59. Unterrainer, K. *et al.* Quantum cascade lasers with double metal-semiconductor waveguide resonators. *Appl. Phys. Lett.* **80,** 3060–3062 (2002).
60. Mahler, L. *et al.* High-performance operation of single-mode terahertz quantum cascade lasers with metallic gratings. *Appl. Phys. Lett.* **87,** 181101 (2005).
61. Ajili, L. *et al.* Loss-coupled distributed feedback far-infrared quantum cascade lasers. *Electron. Lett.* **41,** 419–421 (2005).
62. Williams, B. S., Kumar, S., Hu, Q. & Reno, J. L. Distributed-feedback terahertz quantum-cascade lasers with laterally corrugated metal waveguides. *Opt. Lett.* **30,** 2909–2911 (2005).
63. Demichel, O. *et al.* Surface plasmon photonic structures in terahertz quantum cascade lasers. *Opt. Express* **14,** 5335–5345 (2006).
64. Kumar, S. *et al.* Surface-emitting distributed feedback terahertz quantum-cascade lasers in metal-metal waveguides. *Opt. Express* **15,** 113–128 (2007).
65. Schubert, M. & Rana, F. Analysis of terahertz surface emitting quantum-cascade lasers. *IEEE J. Quant. Electron.* **42,** 257–265 (2006).
66. Dunbar, L. A. *et al.* Small optical volume terahertz emitting microdisk quantum cascade lasers. *Appl. Phys. Lett.* **90,** 141114 (2007).
67. Fasching, G. *et al.* Terahertz microcavity quantum-cascade lasers. *Appl. Phys. Lett.* **87,** 211112 (2005).
68. Chassagneux, Y. *et al.* Terahertz microcavity lasers with subwavelength mode volumes and thresholds in the milliampere range. *Appl. Phys. Lett.* **90,** 091113 (2007).
69. Dhillon, S. *et al.* THz sideband generation at telecom wavelengths in a GaAs-based quantum cascade laser. *Appl. Phys. Lett.* **87,** 071101 (2005).
70. Dhillon, S. *et al.* Terahertz transfer onto a telecom optical carrier. *Nature Photon.* **1,** 411–415 (2007).
71. Adam, A. J. L. *et al.* Beam patterns of terahertz quantum cascade lasers with subwavelength cavity dimensions. *Appl. Phys. Lett.* **88,** 151105 (2006).
72. Orlova, E. E. *et al.* Antenna model for wire lasers. *Phys. Rev. Lett.* **96,** 173904 (2006).
73. Lee, A. W. M. *et al.* High-power and high-temperature THz quantum-cascade lasers based on lens-coupled metal-metal waveguides. *Opt. Lett.* (in the press).
74. Hübers, H.-W. *et al.* Terahertz quantum cascade laser as local oscillator in a heterodyne receiver. *Opt. Express* **13,** 5890–5896 (2005).
75. Bründermann, E. *et al.* Turn-key compact high temperature terahertz quantum cascade lasers: imaging and room temperature detection. *Opt. Express* **14,** 1829–1841 (2006).
76. Ajili, L. *et al.* High power quantum cascade lasers operating at $\lambda \approx 87$ and 130 μm. *Appl. Phys. Lett.* **85,** 3986–3988 (2004).
77. Amanti, M. I., Fischer, M., Walther, C., Scalari, G. & Faist, J. Horn antennas for terahertz quantum cascade lasers. *Electron. Lett.* **43,** 573–574 (2007).
78. Sirigu, L. *et al.* Photonic lattice-based quantum cascade lasers at terahertz frequencies. *Proc. SPIE* **6386,** 63860Z (2006).
79.. Lü, J. T. & Cao, J. C. Monte Carlo simulation of hot phonon effects in resonant-phonon-assisted terahertz quantum-cascade lasers. *Appl. Phys. Lett.* **88,** 061119 (2006).
80. Callebaut, H., Kumar, S., Williams, B. S., Hu, Q. & Reno, J. L. Importance of electron-impurity scattering for electron transport in terahertz quantum-cascade lasers. *Appl. Phys. Lett.* **84,** 645–647 (2004).
81. Vitiello, M. S. *et al.* Measurement of subband electronic temperatures and population inversion in THz quantum-cascade lasers. *Appl. Phys. Lett.* **86,** 111115 (2005).
82. Kröll, J. *et al.* in *OSA Topical Meeting Optical Terahertz Science and Technology, Orlando, Florida* (2007) <http://www.osa.org/meetings/topicalmeetings/OTST/program> .
83. Luo, H. *et al.* Terahertz quantum-cascade lasers based on a three-well active module. *Appl. Phys. Lett.* **90,** 041112 (2007).
84. Huang, F. *et al.* Terahertz study of 1,3,5-trinitro-s-triazine by time-domain and Fourier transform infrared spectroscopy. *Appl. Phys. Lett.* **85,** 5535–5537 (2004).
85. Shen, Y. C. *et al.* Detection and identification of explosives using terahertz pulsed spectroscopic imaging. *Appl. Phys. Lett.* **86,** 241116 (2005).
86. Liu, H.-B., Chen, Y., Bastiaans, G. J. & Zhang, X.-C. Detection and identification of explosive RDX by THz diffuse reflection spectroscopy. *Opt. Express* **14,** 415–423 (2006).
87. Kawase, K., Ogawa, Y., Watanabe, Y. & Inoue, H. Non-destructive terahertz imaging of illicit drugs using spectral fingerprints. *Opt. Express* **11,** 2549–2554 (2003).
88. Siegel, P. H. Terahertz technology in biology and medicine. *IEEE Trans. Microwave Theory Tech.* **52,** 2438–2447 (2004).
89. Bjarnason, J. E., Chan, T. L. J., Lee, A. W. M., Celis, M. A. & Brown, E. R. Millimeterwave, terahertz, and mid-infrared transmission through common clothing. *Appl. Phys. Lett.* **85,** 519–521 (2004).
90. Kumar, S., Williams, B. S., Hu, Q. & Reno, J. L. 1.9 THz quantum-cascade lasers with one-well injector. *Appl. Phys. Lett.* **88,** 121123 (2006).
91. Scalari, G. *et al.* Terahertz emission from quantum cascade lasers in the quantum hall regime: evidence for many-body resonances and localization effects. *Phys. Rev. Lett.* **93,** 237403 (2004).
92. Phillips, T. G. & Keene, J. Submillimeter astronomy. *Proc. IEEE* **80,** 1662–1678 (1992).
93. Gao, J. R. *et al.* in *International Workshop on Low Temperature Electronics (WOLTE 6),* **11** (ESTEC, Noordwijk, The Netherlands, 2004).
94. Gao, J. R. *et al.* A terahertz heterodyne receiver based on a quantum cascade laser and a superconducting bolometer. *Appl. Phys. Lett.* **86,** 244104 (2005).
95. Betz, A. L. *et al.* Frequency and phase-lock control of a 3 THz quantum cascade laser. *Opt. Lett.* **30,** 1837–1839 (2005).
96. Barbieri, S. *et al.* Heterodyne mixing of two far-infrared quantum cascade lasers by use of a point-contact Schottky diode. *Opt. Lett.* **29,** 1632–1634 (2004).
97. Barkan, A. *et al.* Linewidth and tuning characteristics of terahertz quantum cascade lasers. *Opt. Lett.* **29,** 575–577 (2004).
98. Hensley, J. M. *et al.* in *OSA Topical Meeting Optical Terahertz Science and Technology, Orlando, Florida* (2007) <http://www.osa.org/meetings/topicalmeetings/OTST/program>.
99. *Topics in Applied Physics: Terahertz optoelectronics* (ed. Sakai, K.) (Springer, Berlin, 2005).
100. Darmo, J. *et al.* Imaging with a terahertz quantum cascade laser. *Opt. Express* **12,** 1879–1884 (2004).
101. Kim, S. M. *et al.* Biomedical terahertz imaging with a quantum cascade laser. *Appl. Phys. Lett.* **88,** 153903 (2006).
102. Barbieri, S. *et al.* Imaging with THz quantum cascade lasers using a Schottky diode mixer. *Opt. Express* **13,** 6497–6503 (2005).
103. Nguyen, K. L. *et al.* Three-dimensional imaging with a terahertz quantum cascade laser. *Opt. Express* **14,** 2123–2129 (2006).
104. Lee, A. W. M., Williams, B. S., Kumar, S., Hu, Q. & Reno, J. L. Real-time imaging using a 4.3-THz quantum-cascade laser and a 320 × 240 microbolometer focal-plane array. *IEEE Photon. Tech. Lett.* **18,** 1415–1417 (2006).
105. Luo, H., Liu, H. C., Song, C. Y. & Wasilewski, Z. R. Background-limited terahertz quantum-well photodetector. *Appl. Phys. Lett.* **86,** 231103 (2005).
106. Siegel, P. H. & Dengler, R. J. Terahertz heterodyne imaging part II: instruments. *Int. J. Infrared Millimeter Waves* **27,** 631–655 (2006).
107. Dickinson, J. C. *et al.* Terahertz imaging of subjects with concealed weapons. *Proc. SPIE* **6212,** 62120Q (2006).
108. Indjin, D. *et al.* Relationship between carrier dynamics and temperature in terahertz quantum cascade structures: Simulation of GaAs/AlGaAs, SiGe/Si and GaN/AlGaN devices. *Semicond. Sci. Technol.* **20,** S237–S245 (2005).
109. Sun, G., Soref, R. A. & Khurgin, J. B. Active region design of a terahertz GaN/$Al_{0.15}Ga_{0.85}N$ quantum cascade laser. *Superlattices Microstruct.* **37,** 107–113 (2005).
110. Wingreen, N. S. & Stafford, C. A. Quantum-dot cascade laser: Proposal for an ultralow-threshold semiconductor laser. *IEEE J. Quant. Electron.* **33,** 1170–1173 (1997).
111. Hsu, C.-F., O, J.-S., Zory, P. & Botez, D. Intersubband quantum-box semiconductor lasers. *IEEE J. Sel. Top. Quant. Electron.* **6,** 491–503 (2000).
112. Anders, S. *et al.* Electroluminescence of a quantum dot cascade structure. *Appl. Phys. Lett.* **82,** 3862–3864 (2003).
113. Ulbrich, N. *et al.* Midinfrared intraband electroluminescence from AlInAs quantum dots. *Appl. Phys. Lett.* **83,** 1530–1532 (2003).

Acknowledgements

I would like to acknowledge G. Scalari, J. Faist, S. Barbieri, A. Dunbar, A. Tredicucci, Q. Hu, A. W. M. Lee, S. Kumar, P. Siegel, and J. R. Gao, who have provided input and/or figures for this article.